JOURNAL OF MATERIALS SCIENCE 28 (1993) 2283–2288

Characteristics and sintering behaviour of 3 mol % Y_2O_3–ZrO_2 powders synthesized by reaction in molten salts

M. DESCEMOND, C. BRODHAG, F. THEVENOT
Ecole Nationale Supérieure des Mines de Saint Etienne, 158 Cours Fauriel, 42023 Saint Etienne Cedex 2, France

B. DURAND, M. JEBROUNI, M. ROUBIN
Laboratoire de Chimie Minérale 3, URA CNRS no. 116, ISIDT, Université Claude Bernard Lyon I, 43 Boulevard du 11 Novembre 1918, 69622 Villeurbanne Cedex, France

Yttria-stabilized tetragonal zirconia powders have been synthesized by reaction in molten salts at 450 °C. To obtain a Y_2O_3–ZrO_2 solid solution powder, it was necessary to use yttrium salts (not yttrium oxide directly) in molten $NaNO_3$–KNO_3 eutectic. The agglomeration state of the powders depended on their washing conditions. An alcohol-washed powder containing soft agglomerates led to a fine-grained and high-density sintered body.

1. Introduction

Yttria-stabilized tetragonal zirconia (Y-TZP) ceramics have many applications on the basis of their high thermomechanical performances. To obtain fine-grained and highly densified Y_2O_3–tetragonal zirconia ceramics, it is necessary to produce high-purity, very fine, weakly agglomerated and chemically homogeneous Y_2O_3–ZrO_2 solid-solution powders. Several methods resulting from the decomposition of organic or mineral precursors (hydroxide, alcoxide, citrate, etc.) have already been developed. Of the other synthesis methods, the reactions in molten salts have not yet been investigated. The synthesis of zirconium [1] or zirconium diboride [2, 3] in molten chlorides or of barium metazirconate [4] in molten hydroxides has been reported, and monoclinic macrocrystalline zirconia has been prepared by hydrolysis of a molten fluoride mixture [5]. According to Durand [6], double decomposition reactions between a solid alkaline mixed oxide and a molten divalent metal double chloride were likely to lead to finely divided divalent metal mixed oxides. Kerridge and Cancela-Ray [7] studied the reactivity at low temperature between zirconium sulphate and molten alkaline nitrates and showed that under specific conditions, zirconia was formed.

In the present paper, a method of producing 3 mol % Y_2O_3–ZrO_2 solid solution, based on the reaction at 450 °C between zirconium oxychloride and an yttrium source (salt or oxide) in molten nitrates, is presented. The influence of synthesis parameters on the formation of the solid solution, on the powder agglomeration and on its sintering behaviour is reported.

2. Experimental procedure

2.1. Powder preparation

The starting materials were $ZrOCl_2$–$8H_2O$, Y_3O_4Cl, YCl_3, Y_2O_3, $NaNO_3$ and KNO_3. First, zirconium oxychloride was dehydrated at 150 °C by heating the reacting mixture (zirconium oxychloride, yttrium source and nitrates) under a primary vacuum or by heating the oxychloride in air. In this case, the yttrium source and the nitrates were added after dehydration.

The reaction was carried out at 450 °C and took place in accordance with the following equations

$$ZrOCl_2 + NO_3^- \rightarrow ZrO_2 + NO_2^{\square} + Cl^- + 1/2Cl_2^{\square} \quad (1)$$

$$2YCl_3 + 3NO_3^- \rightarrow Y_2O_3 + 3NO_2^{\square} + 3Cl^- + 3/2Cl_2^{\square} \quad (2)$$

$$3Y_3O_4Cl + NO_3^- \rightarrow 3Y_2O_3 + NO_2^{\square} + Cl^- + 1/2Cl_2^{\square} \quad (3)$$

A three-step mechanism in which zirconium oxychloride reacts in the solid state with the molten salt can be proposed to explain the transformation: (1) formation of a chloronitro-complex on the surface of the oxychloride particles, (2) decomposition of this complex and formation of porous zirconia on the surface of the oxychloride particles, and (3) autocatalytic decomposition of the oxychloride leading to the zirconia powder [8].

After reaction, the solid solution was extracted by washing and filtering several times in water. The resulting powder was then dried at 100 °C for several hours (water-washed powders A, B, C, D, E and F). In the case of the alcohol-washed powder G, the last washing was performed with isopropyl alcohol.

The specific conditions of synthesis for each sample are listed in Table I.

2.2. Powder characterization

The identification of the crystallographic phases and

0022–2461

TABLE I Conditions of synthesis of yttria-stabilized zirconia powders

Powder	Yttrium source	Molten medium	Dehydratation conditions	Reaction time (h)	Final washing liquid
A	Y_3O_4Cl	$NaNO_3$–KNO_3	Vacuum	2	Water
B	YCl_3	$NaNO_3$–KNO_3	Vacuum	2	Water
C	Y_2O_3	$NaNO_3$–KNO_3	Vacuum	2	Water
D	YCl_3	$NaNO_3$–KNO_3	Air	2	Water
E	YCl_3	KNO_3	Air	1	Water
F	YCl_3	$NaNO_3$–KNO_3	Air	1	Water
G	YCl_3	$NaNO_3$–KNO_3	Air	2	Isopropyl alcohol

the evaluation of the crystallite sizes was performed by X-ray diffraction (XRD). The particle size and the powder morphology were studied by scanning and transmission electronic microscopies (SEM, TEM) and the porous structure of the agglomerates was investigated by mercury porosimetry and the BET method using nitrogen-gas adsorption. The Y_2O_3 content in each agglomerate was quantitatively examined by X-ray spectrometry and the purity of samples was determined by chemical analysis.

2.3. Sinterability characterization

Compacts for sintering studies were prepared by cold-pressing under 400 MPa. Constant heating-rate dilatometry was performed under an ambient static atmosphere. The heating and cooling rates were 2.5 °C min^{-1}. The green and fired microstructures were observed by SEM.

3. Results and discussion

3.1. The influence of synthesis parameters on the solid-solution formation

The XRD patterns of the water-washed powders A, B, C, D and E are shown in Fig. 1. There was no evidence of yttrium oxide phase whatever the synthesis conditions of the powder. Powders A, B and D were characterized by similar patterns showing tetragonal or cubic phase. After heat treatment at 900 °C, these powders were highly crystalline and their sharp diffraction patterns confirmed the presence of tetragonal phase. For powders C and E, peaks of monoclinic phases were also present. X-ray spectrometry analysis of a 3.5 mol % Y_2O_3–ZrO_2 powder produced in the same way as powder C and containing a similar amount of monoclinic phase showed that the Y_2O_3 content varied from 0.5–4.2 mol %. Powder E had a very low yttrium content (Table II).

As shown by these results, to obtain a Y_2O_3–ZrO_2

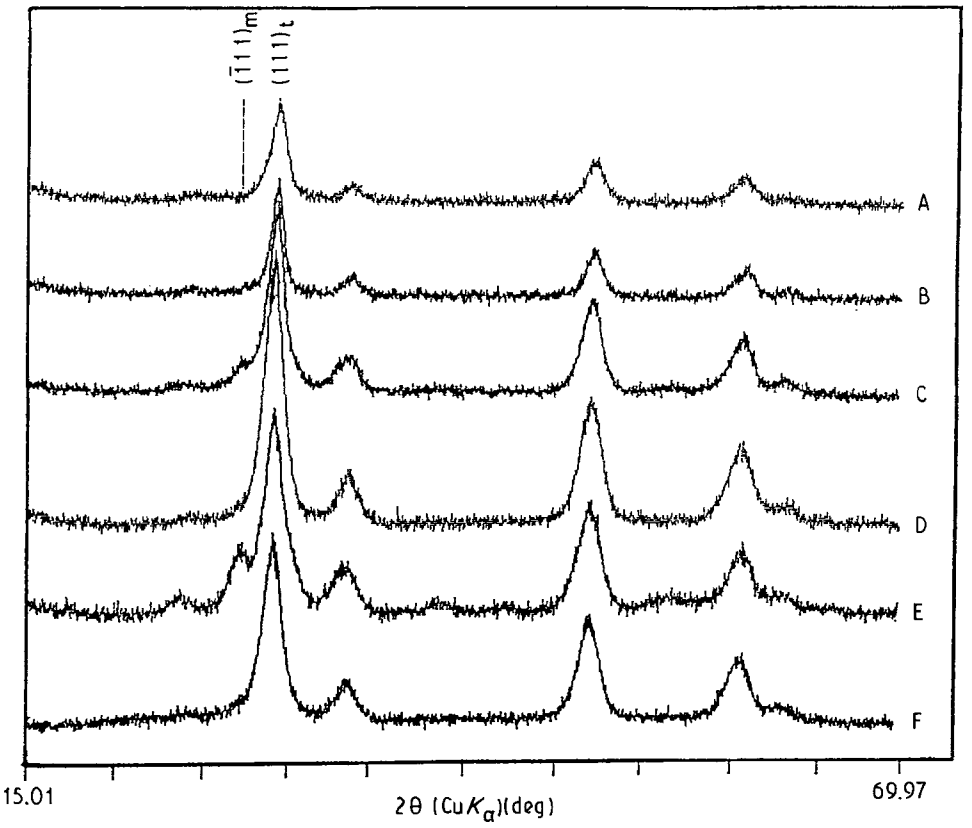

Figure 1 X-ray diffraction patterns of samples A, B, C, D, E and F.

TABLE II Chemical analysis of samples E and F

Sample	Content (wt %)					
	Cl^-	K^+	Na^+	Ca^{2+}	Y^{3+}	Zr^{4+}
E	0.14	0.25	< 0.01	< 0.01	0.01	66.51
F	0.01	0.01	< 0.01	< 0.01	3.90	66.44

solid-solution powder, it was necessary to operate in molten $NaNO_3$–KNO_3 eutectic and to use yttrium salts. With these conditions, a very fine powder was synthesized. This powder consisted of a homogeneous tetragonal phase (Fig. 1), with well-defined yttrium oxide (Table II). On addition of yttrium oxide or in molten KNO_3, the reaction led to a powder with an inhomogeneous composition or with insufficient yttrium content. The conditions of dehydration of zirconium oxychloride had no appreciable influence on the solid-solution formation.

3.2. The influence of the extraction conditions on the agglomeration and sintering behaviour of powders F and G

The water- and alcohol-washed powders F and G were similar. They were constituted by different-sized rod-like agglomerates and by a few small round agglomerates (Fig. 2). TEM observation of the smaller agglomerates or aggregates showed crystallites with a size varying from 6–10 nm in good agreement with X-ray line broadening evaluation (Fig. 3). The specific surface areas of the powders determined by the BET method and calculated in accordance with the TEM crystallite size, were higher than 100 $m^2\ g^{-1}$ (Table III). Large intra-agglomerate pores (from 0.4–0.9 μm for powder G and from 0.7–7.5 μm for powder F) and small inter-crystallite pores (nearly 3.5 nm for both powders) were shown on the pore-size distribution determined using mercury porosimetry (Fig. 4) and the BET method, respectively. The very fine porosity explains the discrepancy between the BET and the mercury porosimetry surface area values (Table III).

The small crystallites ($\leqslant$ 10 nm) observed on the powders were bonded together to form aggregates containing fine inter-crystallite porosity ($\leqslant$ 4 nm). The packing of these aggregates leads to rod-like agglomerates which present larger intra-agglomerates porosity.

During sintering, the two powder compacts exhibited a similar dilatometric behaviour (Fig. 5) characterized by a shrinkage which started at 80 °C and showed a two-step evolution. Table IV indicates that the green densities of the compacts were identical: nearly 50% theoretical density (6.09). The sintered compacts (1500 °C, 1 h) had a density of 98.5% for powder G and only 80% for powder F. Fracture of the sintered powder F compact showed intra-agglomerate sintering. The monoclinic phase content of this compact was significant and higher than that of other compact (the given values are surface values).

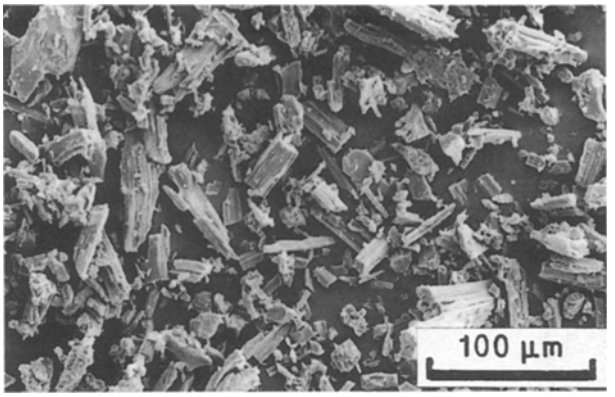

Figure 2 Morphology of the as-received alcohol-washed powder G (scanning electron micrograph).

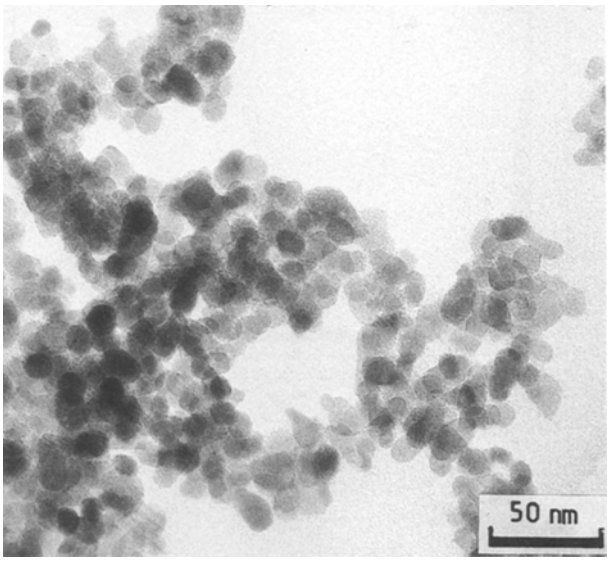

Figure 3 Morphology of the water-washed powder F (transmission electron micrograph).

TABLE III Specific surface areas of powders F and G determined by several methods.

Powder	Specific surface area (m^2/g^{-1})		
	BET method	Microscopy	Hg porosimetry
Water-washed powder F	113	110	42
Alcohol-washed powder G	–	–	17

The weight loss simultaneous to the shrinkage of the compacts was studied by a combination of thermogravimetric analysis (TGA), differential scanning calorimetric analysis (DSC) and Fourier transform– infrared spectroscopy (FT–IR), such that the FT–IR spectra are of the "off" gases of the powder heated during TGA. The matched TGA data, the total absorption FT–IR chromatograms which give the total infrared absorption of all species in the "off" gas as a function of temperature (Figs 6 and 7), and the identification of

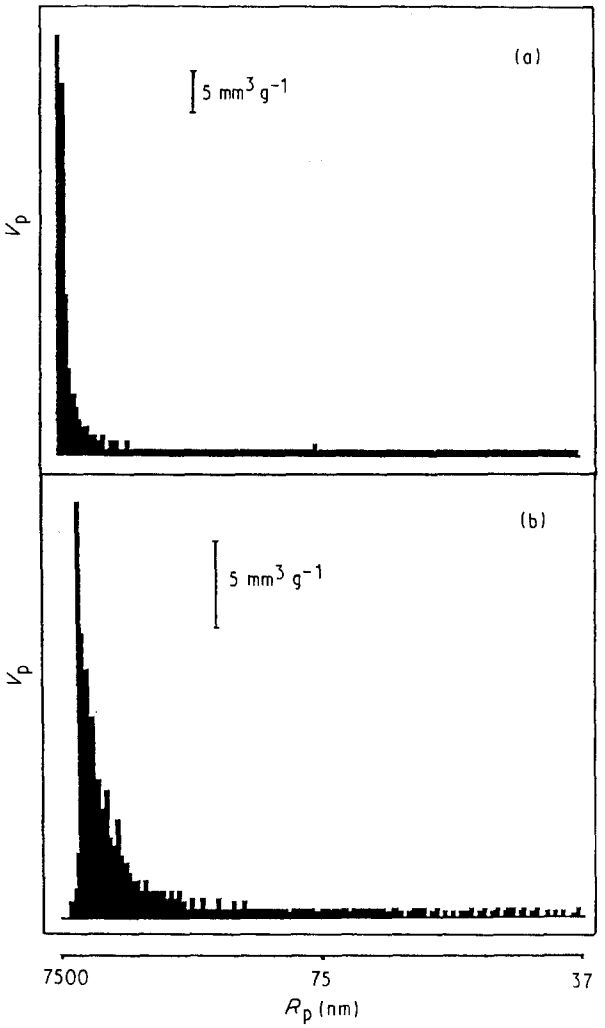

Figure 4 Pore-size distributions of powders (a) F and (b) G from mercury porosimetry.

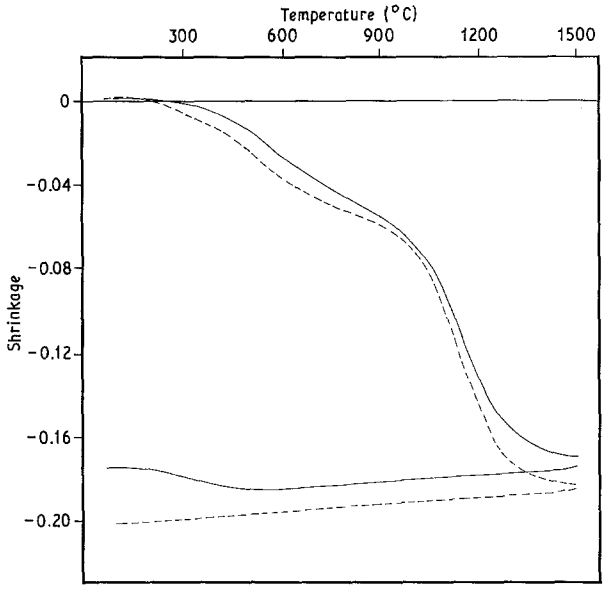

Figure 5 Dilatometric curves of compacts of powders (——) F and (– – –) G (2.5 °C min^{-1}, 1 h at 1500 °C). The curves take into account the dilatation of the zirconia.

these species by individual FT–IR spectra (as shown in Fig. 8), taken at intervals throughout the analysis, revealed a three-step weight loss. The first step was due to the desorption of physisorbed water and carbon dioxide. The second weight loss at higher temperature corresponded to release of chemisorbed species such as CO and CO_2, leading to the formation of surface carbonates. In the case of powder F, the formation of hydroxycarbonates on the hydroxylated surfaces was also possible [9]. The water-washed powder F surface seemed to be proner to chemisorption of these species than that of powder G. The last weight loss occurred in both cases due to the elimination of residual nitrates. The simultaneous emission of CO_2 observed for powder G perhaps results from the decomposition of adsorbed isopropyl alcohol.

According to Bannister [10], the correlation between the volumetric contraction of the compacts and their second and third weight losses suggests that to reduce the porous volume released by the elimination of physisorbed H_2O and CO_2, movement of crystallites is only possible when the chemisorbed species, which act as a binder between adjacent crystallites, are expelled. The diffusion processes also produce intercrystallite sintering and the elimination of the very fine porosity.

TABLE IV Characteristics of the green and sintered bodies (d_{th} 3 mol % Y_2O_3–ZrO_2 = 6.09)

Powder	Green density (400 MPa)	Sintered density (1500 °C, 1 h)	Monoclinic phase content (%)
Water-washed powder F	3.0	4.90	87
Alcohol-washed powder G	3.1	6.04	22

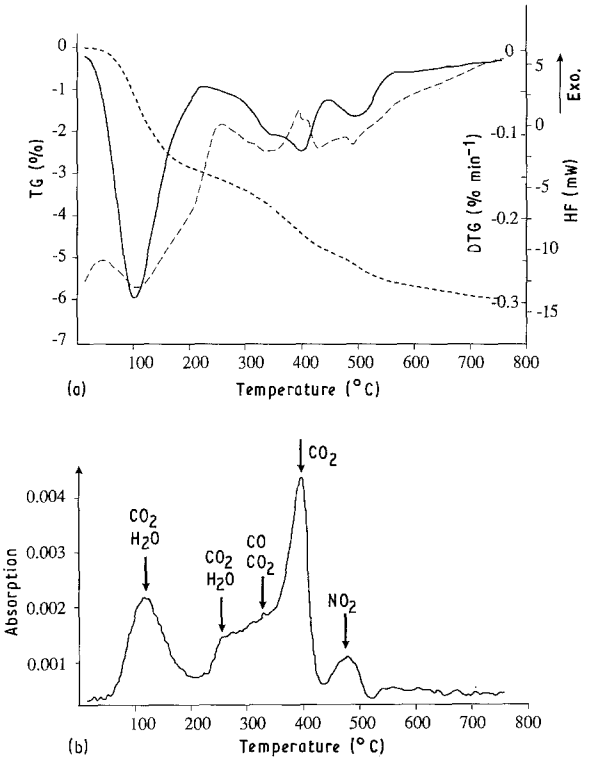

Figure 6 Thermal analysis of water-washed powder F: (a) (- - -) thermogravimetric data (TG), (——) derivative of thermogravimetric data (DTG), (– – –) differential scanning calorimetry data (HF), and (b) FT–IR chromatogram (absorption).

Kaliszewski and Heuer [11] proposed mechanisms to explain the effects of the washing medium on the powder agglomeration. In water-washed powder F, adjacent particles are bonded by water and terminal surface hydroxyl groups. During drying, this hydrogen bonding favours the close approach of particles leading to Zr–O–Zr bond formation and consequently to hard agglomerates. In alcohol-washed powder, this bonding is inhibited by the surface isopropoxy groups leading to the formation of soft agglomerates. During alcohol-washed powder compaction, the porous agglomerates are broken and they lead to a uniformly packed compact with intra-agglomerates and inter-crystallites porosities. The water-washed powder compact exhibits, in addition, large inter-agglomerates pores which are not eliminated during sintering and limit the sintered density. Ready *et al.* have made the same observations [12].

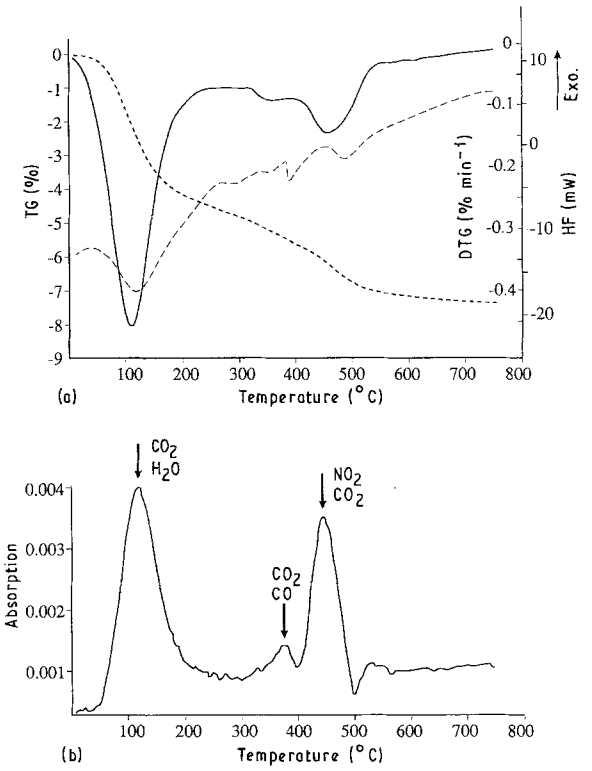

Figure 7 Thermal analysis of alcohol-washed powder G: (a) (- - -) thermogravimetric data (TG), (——) derivative of thermogravimetric data (DTG), (– – –) differential scanning calorimetry data (HF), and (b) FT–IR chromatogram (absorption).

The stresses applied to a grain by its neighbouring grains and, consequently, the stabilization of tetragonal zirconia, increase with the sintered density [13]. By limiting the densification, the zirconia powder agglomeration indirectly affects the stabilization of tetragonal zirconia.

Sintering of the alcohol-washed powder G at 1500 °C leads to a fine-grained ($\approx$ 0.5 μm) and high-density (6.04) sintered body of 3 mol % Y_2O_3–ZrO_2. The sinterability of the very fine powders produced by the method presented in this paper is similar to, but not higher than, the sintering behaviour of powders of lower surface area ($< 40\ m^2\ g^{-1}$) industrially synthesized by the sublimation hydrolysis method [14].

4. Conclusions

The reaction at 450 °C between zirconium oxychloride and an yttrium salt in a molten $NaNO_3$–KNO_3 mix-

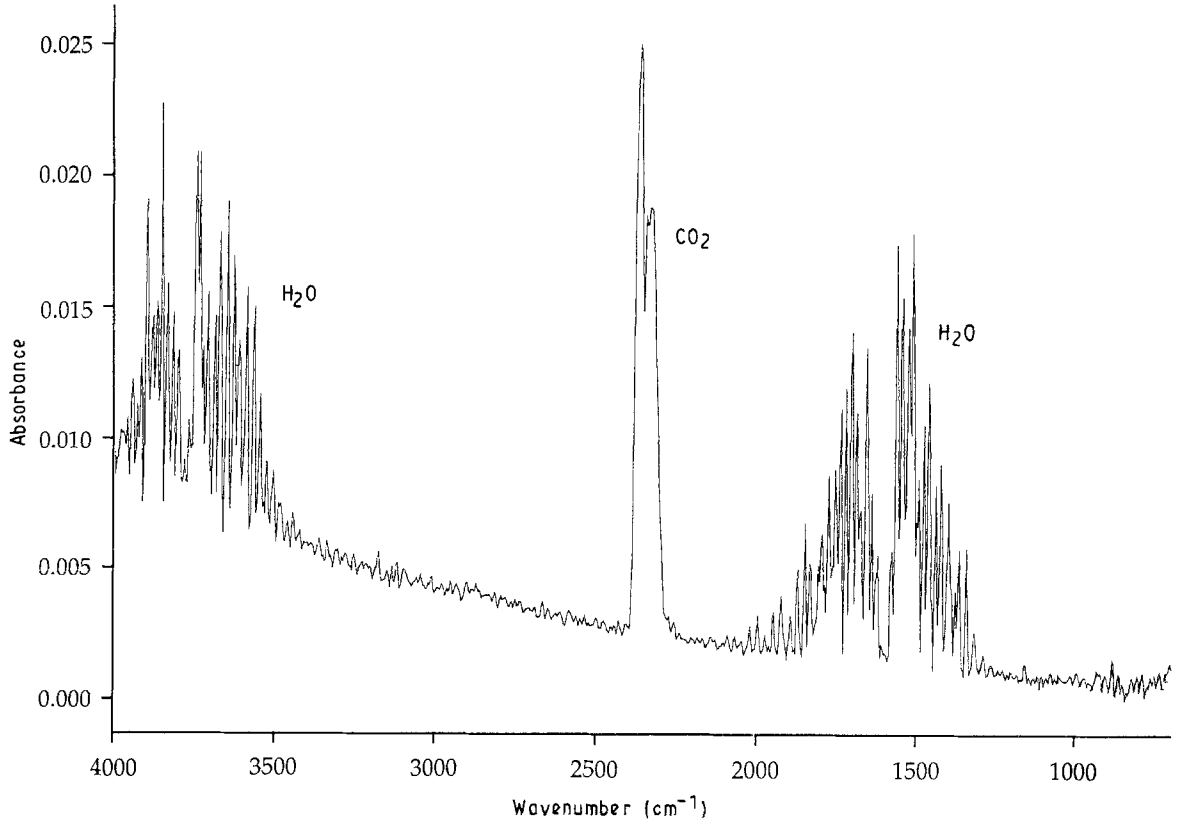

Figure 8 FT–IR spectrum of "off" gases from the water-washed powder F at 130 °C.

ture, produces a very fine 3 mol % Y_2O_3–ZrO_2 powder. The state of agglomeration of these powders depends on the final washing liquid used during their processing. An alcohol-washed powder containing soft agglomerates leads to a fine-grained and high-density sintered body.

References

1. A. J. BECKER and D. R. CAREATTI, (Aluminium Co. of America) US Pat. 4285 724 (Cl. 75-84.4; C22B34/14), 25 August 1981, Appl. 94, 15 November 1979; 8 pp.
2. A. J. BECKER, *Proc. Electrochem. Soc.* **83** (7) (1983) 65.
3. *Idem*, (Aluminium Co. of America) US Pat. 4414, 188 (Cl. 423-297: C01B35/04), 8 November 1983, Appl. 371, 23 April 1982; 8 pp.
4. A. ARENDT (General Electric Co.), US pat. 4374 117 (Cl. 423-593; C01G23/00), 15 February 1983, Appl. 320, 12 November 1981; 6 pp.
5. C. B. FINCH and P. F. BECHER, *J. Crystal Growth* **60** (1982) 321.
6. B. DURAND, in "Ceramic Powders" Ed. P. Vincenzini (Elsevier Science, Amsterdam, 1983) p. 413.
7. D. H. KERRIDGE and J. CANCELA-RAY, *J. Inorg. Nucl. Chem.* **39** (1977) 405.
8. M. JEBROUNI, Thesis 169-90, University Lyon I (1990).
9. H. KNÖZINGER, in "Advances in Catalysis", Vol. 25 (Academic Press, New York, 1976) p. 184.
10. M. J. BANNISTER, Tech Rept. AAEC/TM 464 (1968).
11. M. S. KALISZEWSKI and A. H. HEUER, *J. Amer. Ceram. Soc.* **73** (1990) 1504.
12. M. J. READY, R.-R. LEE, J. W. HALLORAN and A. H. HEUER, *ibid.* **73** (1990) 1499.
13. F. F. LANGE, *J. Mater. Sci.* **17** (1982) 225.
14. M. DESCEMOND, C. BRODHAG, F. THEVENOT, P. HOMERIN and E. ROTHMAN. *Ceramica Acta* **0** (1989) 180.

Received 13 September 1991
and accepted 2 September 1992